J Mol Model (2012) 18:3563–3576
DOI 10.1007/s00894-012-1354-y

ORIGINAL PAPER

Mechanisms and kinetics of thiotepa and tepa hydrolysis: DFT study

Hedieh Torabifard · Alireza Fattahi

Received: 9 November 2011 / Accepted: 3 January 2012 / Published online: 14 February 2012

Abstract N,N′,N″-triethylenethiophosphoramide (Thiotepa) and its oxo analogue (Tepa) as the major metabolite are trifunctional alkylating agents with a broad spectrum of antitumor activity. In vivo and vitro studies show alkylation of DNA by Thiotepa and Tepa can follow two pathways, but it remains unclear which pathway represents the precise mechanism of action. In pathway 1, these agents are capable of forming cross-links with DNA molecules via two different mechanisms. In the first mechanism, the ring opening reaction is initiated by protonating the aziridine, which then becomes the primary target of nucleophilic attack by the N7-Guanine. The second one is a direct nucleophilic ring opening of aziridyl group. Thiotepa and Tepa in pathway 2, act as a cell penetrating carrier for aziridine, which is released via hydrolysis. The released aziridine can form a cross-link with N7-Guanine. In this study, we calculated the activation free energy and kinetic rate constant for hydrolysis of these agents and explored interaction of aziridine with Guanine to predict the most probable mechanism by applying density functional theory (DFT) using B3LYP method. In addition, solvent effect was introduced using the conductor-like polarizable continuum model (CPCM) in water, THF and diethylether. Hyperconjugation stabilization factors that have an effect on stability of generated transition state were investigated by natural bond order (NBO) analysis. Furthermore, quantum theory of atoms in molecules (QTAIM) analysis was performed to extract the bond critical points (BCP) properties, because the electron densities can be considered as a good description of the strength of different types of interactions.

Keywords Anticancer drugs · DFT · Hydrolysis · Kinetic study · Thiotepa and Tepa

Introduction

Although the alkylating agent N,N′,N″-triethylenethiophosphoramide (Thiotepa) (Fig. 1), represents one of the oldest chemotherapeutic agents with continuing clinical utility [1–5] in high dose combination regimens for breast, ovarian, bladder cancers and other solid tumors [6–9], little is known about the mechanism by which it alkylates DNA. Despite many years of experience with Thiotepa, pharmacological data are incomplete. In recent years greater insight has been obtained into the metabolism of Thiotepa, but there is still a gap between the alkylating activity and mechanism of reaction [6].

Metabolic studies of Thiotepa resulted in the identification of its oxo analogue (Tepa) as the major metabolite which is formed after oxidative desulfuration of Thiotepa in the liver by cytochrome P450 (Fig. 1) [6–9]. Thiotepa and Tepa have been classified as trifunctional alkylating agents (which contain three aziridinyl functionalities) that are proposed to induce cancer cell death by formation of cross-links within DNA [10–13]. In vivo and vitro studies show that the alkylation of DNA by Thiotepa and Tepa can proceed via two different pathways, but the precise mechanism of action still remains unclear [6–8]. These two anticancer drugs react with DNA, typically with Guanine at position N7, although others alkylation sites are reported [14, 15]. Alkylation is followed by other reactions, depurination being a typical example [16].

Electronic supplementary material The online version of this article (doi:10.1007/s00894-012-1354-y) contains supplementary material, which is available to authorized users.

H. Torabifard · A. Fattahi (✉)
Department of Chemistry, Sharif University of Technology,
P.O. BOX:11365-9516,
Tehran, Iran
e-mail: fattahi@sharif.edu

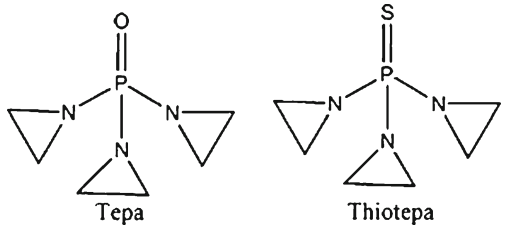

Fig. 1 The structure of thiotepa and tepa

A first necessary step in the alkylating agent activity is considered to be its interaction with DNA, either directly or after metabolic activation. Following Miller's theory, sites that potentially could interact with electrophilic species are the DNA nucleophilic centers: nitrogen and oxygen atoms of pyrimidine and purine bases [17]. In addition to the chemical nature of the reactive species, the specificity of the reactions at the different sites strongly depends on the nucleophilicity of the DNA centers and on steric factors. The most nucleophilic sites are endocyclic nitrogen atoms such as N3 and N7 guanine and adenine, while exocyclic base oxygen is less nucleophilic [18]. Guanine N7, exposed in the major groove of normal helical DNA, is more accessible and hence more able to react with electrophiles than the N3 position of adenine oriented to the minor groove. By similar reasoning, highly nucleophilic sites such as N1 of adenine and N3 of cytosine do not react extensively because of steric hindrance [19]. Furthermore, the active sites of DNA bases commonly have been rationalized in terms of hard-soft reactivity principles [20–22]. Hard alkylating agents (defined by small size, positive charge, and low polarizability) display increased reactivity with hard oxygen nucleophilic in DNA while soft (large, uncharged and Polarizable) alkylating agents favor reactions at the softer nitrogens. Therefore, the alkylation of DNA usually takes place on N7–Guanine [17].

As mentioned previously, two pathways are suggested. In pathway 1, these agents are capable of forming cross-links with DNA molecules according to two different mechanisms. In the first mechanism, the ring opening reaction is initiated by protonation of the aziridine, which then becomes the main target of nucleophilic attack by the N7 Guanine of DNA [23]. The second one is the direct nucleophilic ring opening of aziridinyl groups. The reactivity of aziridinyl group is because of presence of electron withdrawing substituents (–P=S and –P=O substituents in Thiotepa and Tepa), which causes it to react with nucleophiles to produce ring–opened products [24].

In pathway 2, Thiotepa acts as a cell–penetrating carrier for aziridine, which is released after hydrolysis. The released aziridine can react with DNA to form the stable Guanine adduct in the DNA chain [25, 26]. These two pathways are presented in Fig. 2. On the basis of DNA adducts and the rate of formation of aziridine by hydrolysis in vitro, Thiotepa is calculated to be a lipophilic, stabilized form of aziridine which serves as a cell–penetrating carrier of aziridine [25].

In fact Thiotepa rapidly enters cells by passive diffusion [27], where hydrolysis of Thiotepa can take place chemically or enzymatically to release aziridine. Thus, more aziridine may be delivered to DNA in cells than if the aziridine had been administered directly. Release of aziridine inside the cell may explain why Thiotepa and Tepa have similar toxicities against cancer cell [28, 29]. Furthermore, for phosphoramidates (one P-N and two P-O bonds), it is known that P-N bond hydrolysis can be catalyzed biotically [30].

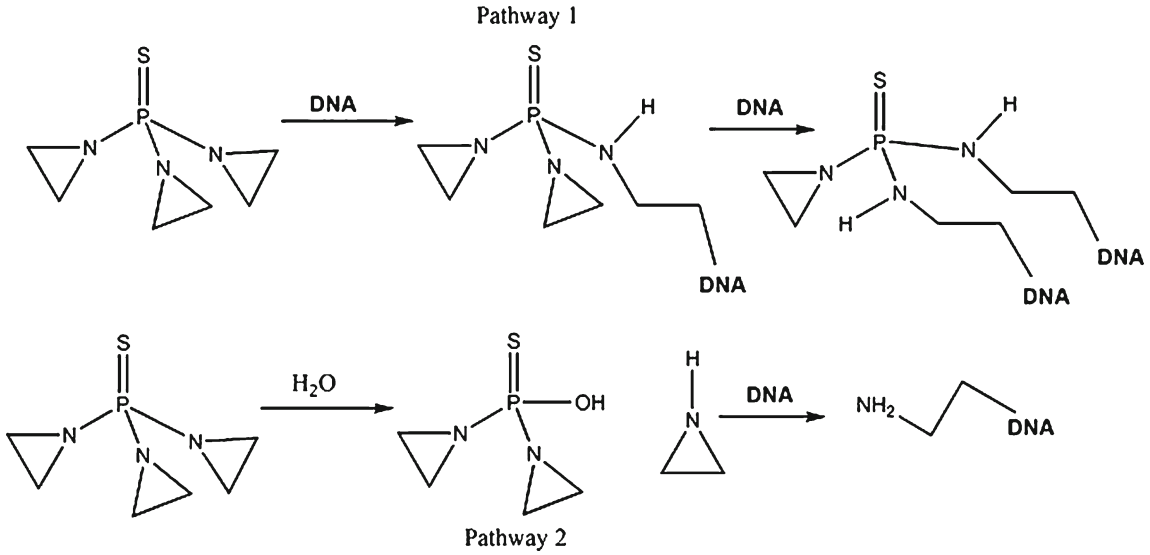

Fig. 2 Possible interaction of thiotepa with DNA. Pathway 1: formation of cross links between thiotepa and DNA. Pathway 2: thiotepa as a prodrug for aziridine

Therefore, we are aware of possible enzymatic P-N bond hydrolysis for these two anticancer agents in the cells, but in this study the enzymatic effect on rate of reactions are given up and only the chemical reactions are investigated. Lastly, it is well established that the rate–limiting step for reaction of aziridine with N7-Guanine is the aziridine ring opening.

In this study, we investigate the mechanisms of P-N bond hydrolysis in Thiotepa and Tepa using density functional theory (DFT). First, Gibbs free energies of activation ($\Delta G^{\#}$) were calculated, then the rate constants k [31] were obtained on the basis of the transition state theory:

$$k = \frac{k_B T}{h} \times e^{-\frac{\Delta G^{\neq}}{k_B T}}, \quad (1)$$

where k_B, h and T represent Boltzmann constant, the Planck's constant, the absolute temperature, respectively. Transition state theory is based on the assumption that reactants and transition states form a thermal equilibrium. Its validity in biocatalysis was proven experimentally by the development of catalytic antibodies and theoretically by the success of empirical valence bond (EVB) method [32]. Because biochemical reactions do not take place in vacuum, solvation effects had to be incorporated by the solvent reaction field method of Tomasi and co-workers [33] and a cluster–continuum solvation model [34]. In addition, to complete investigation on these drugs' mechanisms, the ring opening mechanism of aziridine also is studied computationally.

Computational methods

Initial search of minima on the potential energy surface of free Guanine and/or reactants at the relative energy range of 10 kcal mol^{-1} were carried out using the MMFF force field by using Spartan software [35]. The most stable conformers were optimized by the density functional (DFT) method using Becke3 (B3) exchange [36] and Lee, Yang, and Parr (LYP) correlation [37] potentials, in connection with the 6-311++G(d,p) orbital basis set. The analytical harmonic vibrational wave numbers for all structures were positive values, confirming that the local minima on the potential energy surface had been found. Transition states were explored employing the quadratic berny algorithm. The transition state structures have a negative value for the analytical harmonic vibrational wave number.

The solvation free energies were obtained theoretically using a continuum solvation method. The polarizable continuum model (PCM) [38] was applied using the conductor-like polarizable continuum variant (CPCM) [39]. CPCM calculations were performed as single points (without optimization) on the gas phase geometries, since this has been shown to give better results than re-optimization [40]. The water, THF and diethylether solvent were modeled with the dielectric constants 80, 8, and 4 to simulate the condition of cells [41–44]. Here, we have applied DFT calculations in combination with a cluster-continuum model to account for solvent effects, which has been shown to yield satisfactory solvation energies [45–47].

Natural bond order (NBO) analysis was carried out using the B3LYP functional and the 6-311++G (d,p) basis set. In this context, a study of hyperconjugative interactions has been completed. Hyperconjugation may be given as a stabilizing effect that arises from an overlap between an occupied orbital with another neighboring electron deficient orbital when these orbitals are properly oriented. This bonding–antibonding interaction can be quantitatively described in terms of the NBO approach that is expressed by means of the second-order perturbation interaction energy ($E^{(2)}$) [48–52]. This energy represents the estimation of the off-diagonal NBO Fock matrix elements. It can be deduced from the second-order perturbation approach [52]:

$$E^{(2)} = \Delta E_{ij} = q_i \frac{F(i,j)^2}{\varepsilon_i - \varepsilon_j}, \quad (2)$$

where, q_i is the donor orbital occupancy, ε_i; ε_j are diagonal elements (orbital energies) and F (i, j) is the off-diagonal NBO Fock matrix element.

Furthermore, electron densities $\rho(r)$ and Laplacians $\nabla^2 \rho(r)$ of various interactions at bond critical points have been calculated at the 6-311++G (d,p) level using Bader's theory of atoms in molecules (AIM) [52, 53]. AIM is a very useful tool in analyzing hydrogen bonds and interactions, with a large electronic density at the critical point. In this paper, we calculated the electron density topological properties of our systems using the AIM2000 program [54]. According to the AIM theory, the presence of a hydrogen bond like any chemical bond must correspond to the existence of a bond path between the donor and the acceptor atoms containing the bond critical point (BCP), in topological analysis of the electron density distribution. Laplacian of $\rho(r)$ is related to the bond interaction energy by a local expression of the viral theorem [55]:

$$\left[\frac{\hbar^2}{4m}\right] \nabla^2 \rho(r) = 2G(r) + V(r), \quad (3)$$

where $G(r)$ is the electronic kinetic energy density and $V(r)$ is the electronic potential energy density. A negative$\nabla^2 \rho(r)$ shows the excess potential energy at bond critical point (BCP). It means that electronic charge is concentrated in the inter-nuclear region, and therefore, shared by two nuclei. This is the case in all shared electron (covalent) interactions. A positive $\nabla^2 \rho(r)$, at a BCP reveals that the kinetic energy

contribution is greater than that of potential energy, and shows depletion of electronic charge along the bond path. This is the case in all closed-shell electrostatic interactions [56, 57]. Furthermore, the electronic energy density H(r) at BCP is defined as H(r)=G(r)+V(r). The sign of $H(r)$ determines whether the accumulation of charge at a given point of r is stabilizing ($H(r)<0$) or destabilizing ($H(r)>0$). The bond energies $\mathbf{E_X}$ were calculated by using the following equation:

$$E_x = 1/2V_{(r)} \qquad V_{(r)} = 1/4\nabla^2\rho(r) - 2G(r) \quad (4)$$

Finally, the criterion nature of bonds evaluated by means of –G(r)/V(r) ratio. When –G(r)/V(r)>1 the interaction is noncovalent, while for 0.5<–G(r)/V(r) <1 it is partly covalent [58, 59]. Moreover, Rozas et al. have developed a new classification of the interactions [60]. Weak interactions exhibit positive values for both $\nabla^2\rho(r)$ and H(r), for medium interactions $\nabla^2\rho(r)>0$ and H(r)<0, and for strong interactions both $\nabla^2\rho(r)$ and H(r) are negative. We use the E_X values and these criteria to characterize different interactions considered in this study. It is important to note that the AIM analysis is more practicable for hydrogen bonds but in the case of other interaction it can be useful.

Results and discussion

Tautomerization of guanine nucleobase

As common with nucleic acid bases, the Guanine has several possible tautomers. Firstly, it is essential to identify all of the minima on the potential energy surface for Guanine in the range of 10 kcal mol^{-1}. Therefore, all six tautomers which are presented in Fig. 3 were optimized by using B3LYP/6-311++G (d,p) to choose the best tautomers for calculations. The electronic energies, Gibbs free energies and dipole moments of these tautomers are given in Table 1. The relative electronic energies and relative Gibbs free energies indicate that structure four is the most stable tautomer which was selected for the next calculations.

First step: hydrolysis of thiotepa and tepa

To predict the reaction rate for Thiotepa and Tepa hydrolysis in the acidic and physiological pH, the potential reaction mechanisms were investigated computationally. Complete change of a reactant to its product may happen via more than just a transition state (TS). As a result, all credible reaction mechanisms should be investigated to maximize prediction exactness. The reaction paths which have the lowest free energy of activation govern the total reaction rate. For hydrolysis of P-N bond in tetra-coordinate phosphorous compound like Thiotepa and Tepa, four general mechanisms have previously been presented to be theoretically possible in physiological pH (see Fig. 4 for more details) [61]: (1) an elimination–addition mechanism (stepwise dissociative mechanism) which has a tri-coordinate intermediate, (2) an addition–elimination mechanism (stepwise associative mechanism) which has a penta-coordinate intermediate, (3) a concerted front side mechanism, and (4) a concerted backside mechanism, with one penta-coordinate transition state in which water attacks the central phosphorous atom at the same time as one of the aziridine substituents is leaving.

The reported pH for cancer cells is in the pH range of 4-6 [62]. Therefore, the protons at low pH of cancer cells can catalyze the reaction. Proceeding of acid–catalyzed hydrolysis of tetra-coordinate phosphorous amides is via a

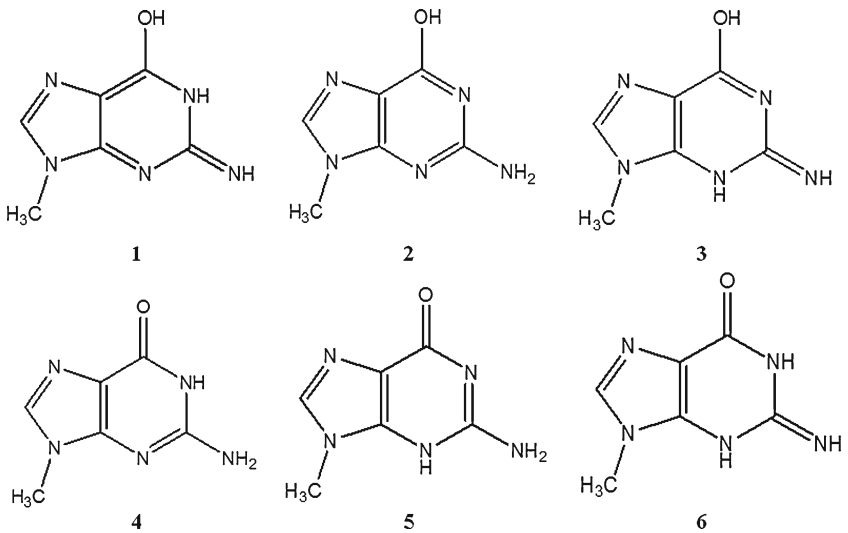

Fig. 3 Optimized structure of tautomers of guanine at B3LYP/6-311++G(d,p)

Table 1 B3LYP/6-311++G (d,p) absolute energies (E, in a.u), Gibbs free energies (G, in a.u), relative energies (ΔE, in kcal mol^{-1}), relative Gibbs free energies (ΔG, in kcal mol^{-1}), and dipole moments of the all tautomers of Guanine

Tautomers	E	ΔE	μ	G	ΔG
1	−581.844579	22.0	4.6	−581.891229	21.6
2	−581.877349	1.5	4.2	−581.922963	1.7
3	−581.829137	31.7	9.7	−581.876060	31.1
4	−581.879678	0	7.4	−581.925667	0
5	−581.848861	19.3	13.4	−581.894925	19.3
6	−581.855785	15.0	10.1	−581.900836	15.6

backside attack mechanism, (Fig. 5) [61, 63–66] or via dissociative mechanism with a tri-coordinate intermediate (Fig. 6). The dependence of the rate constant on proton activity is reflected by protonation of the P-N bond which greatly increases hydrolysis rates because the nitrogen containing substituent becomes a better leaving group [67].

Dissociative stepwise mechanism

In this mechanism, the ionic intermediate is formed by the heterolytic dissociation of the P-N bond (see Fig. 4 for more details). This dissociation reaction is considered as rate limiting step, which is predicted to have a $\Delta_r G_{(g)}$ of 79.0 kcal mol^{-1} and 83.0 kcal mol^{-1} for Thiotepa and Tepa in gas phase, respectively. As obvious the free energy of the transition state must be equal to or higher than that of the intermediate, therefore their free energy of activation should be≥79.0 and 83.0 kcal mol^{-1} and thus meaningfully greater than that of all the other mechanisms considered herein (Fig. 4), consequently this mechanism was ruled out without further determination of the transition states.

Associative stepwise mechanism

In the first transition state of this mechanism for Tepa (TS1,$\Delta G_{(g)}^{\#}$=32.8 kcal mol^{-1}, see Fig. 7 for more details), the direct proton transfer to the oxygen atom which is double-bonded to the central phosphorous atom, proceeds by the attacking nucleophile H_2O, while the remaining hydroxyl group forms a new single covalent bond with phosphorous. For the penta-coordinate intermediate (INT, $\Delta_r G_{(g)}$=29.6 kcal mol^{-1}, Fig. 7), a psuodorotation mechanism, could not be found, possibly because of steric hindrance imposed by the bulky aziridine substituents. Rather, the proton on oxygen atom transfers through a second transition state (TS2, $\Delta G^{\#}_{(g)}$ = 11.3 kcal mol^{-1}, Fig. 7), to form phosphoric diaziridine, as the product. It is important to note that the second step is considered as a fast step, it means that the first step in which a proton from nucleophile H_2O transfers to oxygen atom on Tepa is the rate limiting step.

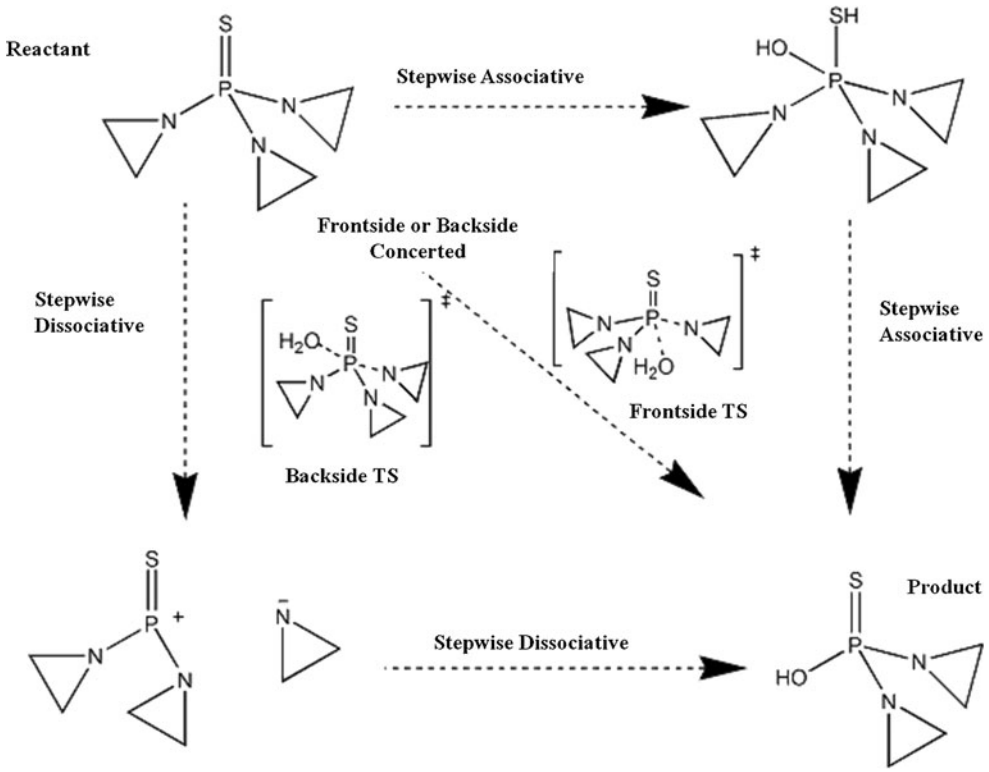

Fig. 4 Mechanisms of P-N bond hydrolysis in physiological pH

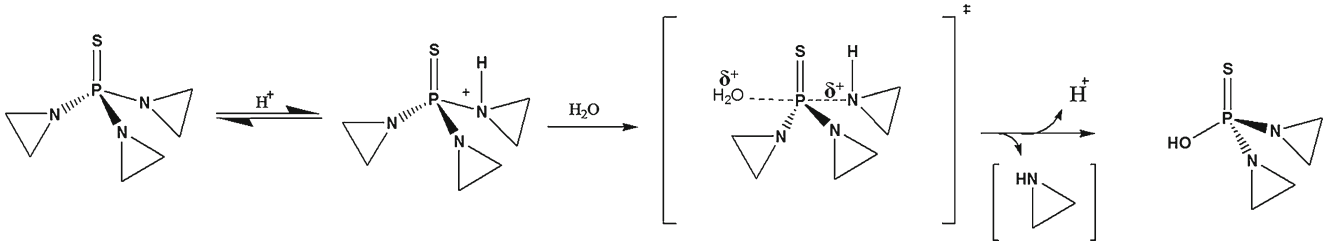

Fig. 5 Concerted backside mechanism of P-N bond hydrolysis in acidic pH

On the other hand, similar calculations were computed for Thiotepa (TS1, $\Delta G^{\#}_{(g)}$=57.1 kcal mol^{-1}, Fig. 7), (INT, $\Delta_r G_{(g)}$ =27.6 kcal mol^{-1}, Fig. 7), (TS2, $\Delta G^{\#}_{(g)}$ = 21.1 kcal mol^{-1}, Fig. 7). The value of $\Delta G^{\#}_{(g)}$ for TS1 indicates that this mechanism is not favorable for thio analogue. A comparison on the gas-phase energies of the neutral and protonated forms of these agents, which are presented in Table 2, shows that the N-protonated form of Thiotepa is more stable than the S-protonated form, while in the case of Tepa the O-protonated form of Tepa appears to be more stable than the N-protonated form. Moreover, hydrogen and oxygen atoms are hard species, while the sulfur atom is soft specie, and hence interaction of hydrogen and oxygen atoms is more favorable than that of hydrogen and sulfur atoms. In conclusion, the associative mechanism is less probable for Thiotepa, while the Tepa proceeds via this mechanism with high probability. The schematic profiles of the potential energy surfaces of the Tepa and Thiotepa hydrolysis in this mechanism are presented and compared in Fig. 8.

These results are confirmed by the AIM analysis. Results obtained for electron densities ρ(r) and their Laplacians $\nabla^2 \rho(r)$, kinetic energy densities G(r), potential energy densities V(r), and electronic energy densities H(r), bond energies of hydrogen bonds and -G(r)/V(r) ratio at the BCPs calculated at B3LYP/6-311++G (d,p) level of theory for the Thiotepa and Tepa are given in Table 1S in Supporting information. (The tables presented in Supporting information are denoted by S.)

As shown in Table 1S, in reactant there is weak hydrogen bond ($\nabla^2 \rho(r)$ and H(r) >0) between H atom of water molecule with O atom on Tepa (3.9 kcal mol^{-1}), while there is no interaction in reactant between S atom on Thiotepa and H atom of water molecule and in first transition state there is very weak interaction between S atom and H atom of water molecule (2.9 kcal mol^{-1}), while there is medium interaction ($\nabla^2 \rho(r)$ >0 and H(r) <0) between O and H atoms in Tepa (49.7 kcal mol^{-1}).

In addition, natural bond orbital analysis shows that the first transition state in Tepa is much more stable than that in Thiotepa due to the second order energy of LP→BD* (n→σ*) and BD→BD* (σ→σ*) type of interactions (see Table 2S). It is important to note that the negligible values in the case of Thiotepa can be considered as NBO analysis errors. In the case of second transition state, there are interactions between $n_{N\ (leaving\ group)} \rightarrow \sigma^*_{O\ (Tepa)\text{-}H1}$ (118.5 kcal mol^{-1}) in Tepa and $n_{N\ (leaving\ group)} \rightarrow \sigma^*_{S\ (Thiotepa)\text{-}H1}$ (30.5 kcal mol^{-1}) in Thiotepa (H1 and H2 are shown in Fig. 7).

In conclusion, the results of NBO and AIM analyses indicate that the associative stepwise mechanism is not the probable mechanism for Thiotepa, however it can be considered as a logical mechanism for Tepa.

Concerted frontside mechanism

In the concerted front-side mechanism, a proton is transferred to the nitrogen atom within the leaving aziridine by the attacking water molecule to form the transition state ($\Delta G^{\#}_{(g)}$= 61.8 kcal mol^{-1} for Thiotepa, $\Delta G^{\#}_{(g)}$ =62.3 kcal mol^{-1} for Tepa, see Fig. 9 for more details). The P-N bond is 1.69 Å and 1.68 Å in the ground state, which is lengthened to 2.54 Å and

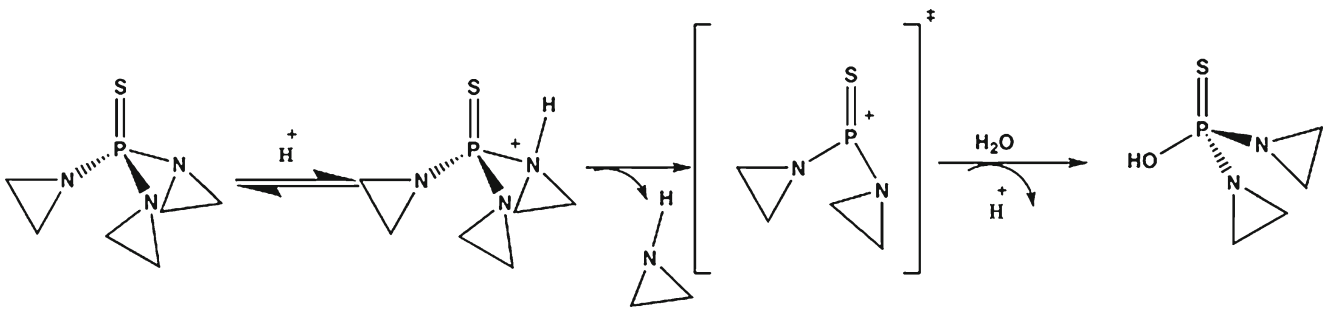

Fig. 6 Dissociative mechanism of P-N bond hydrolysis in acidic pH

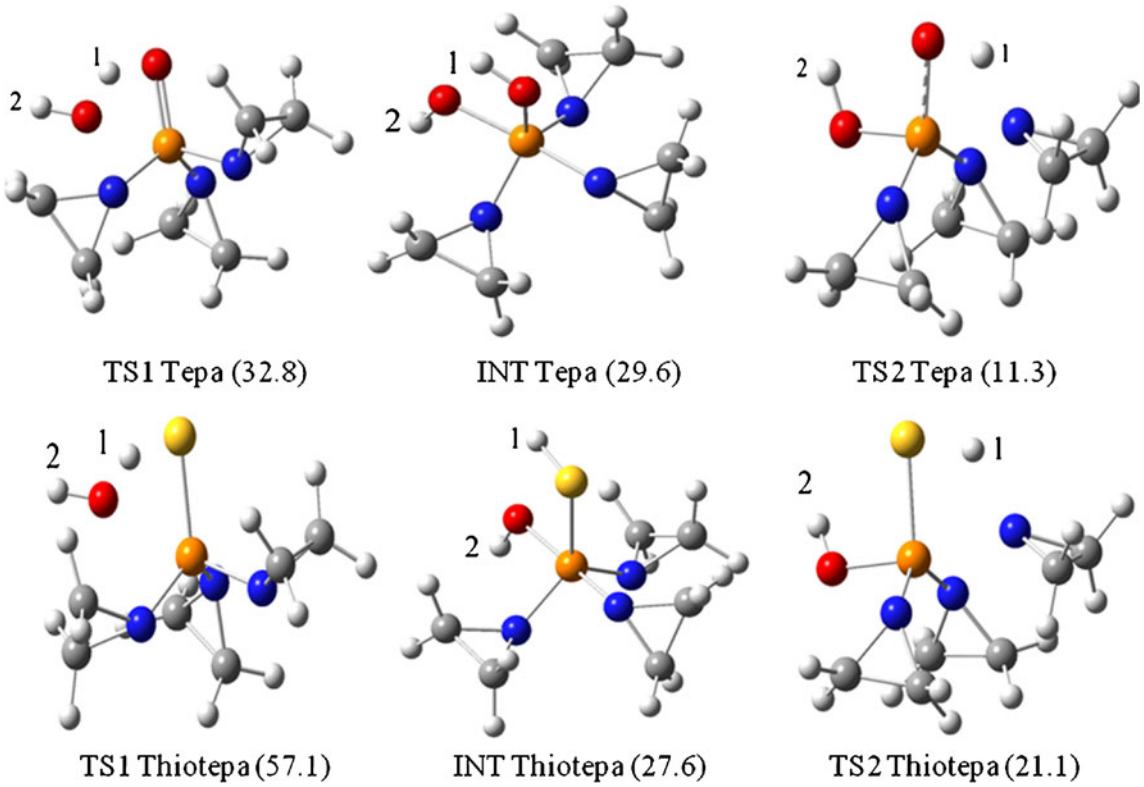

Fig. 7 Optimized geometries of stationary points for tepa and thiotepa hydrolysis in gas phase in associative stepwise mechanism. Values in parentheses are Gibbs free energies of activation in kcal mol^{-1} for transition states and the intermediate in gas phase at 298 K

2.57 Å in the transition state for Thiotepa and Tepa, respectively. On the other hand, a covalent P-O bond is formed by the resulting hydroxide ion which approaches the phosphorous atom. As mentioned in dissociative mechanism, the values of the activation free energies for these two agents revealed this fact that the concerted front-side mechanism is not kinetically favorable mechanism in the gas phase. Therefore, more calculations in this regard were abandoned.

Concerted backside mechanism

In the concerted backside mechanism for Thiotepa and Tepa (Fig. 4) water molecule as a nucleophile attacks the central phosphorous atom on one side to form a covalent P-OH bond. On the opposite side of the phosphorous, the leaving aziridine group which is a potent proton acceptor accepts proton from the environment. It is important to note that the proton transfers with the cellular environment consider as fast step. The activation free energy of this mechanism in gas phase for Thiotepa (14.0 kcal mol^{-1}, Fig. 10) and Tepa (14.5 kcal mol^{-1}, Fig. 10) are nearly 48 kcal mol^{-1} lower than that for the front side mechanism, respectively. Murray et al. have reported that the phosphorus of $O{=}PCl_3$ has strong positive region (positive σ-hole). Hence, it acts as a

Table 2 B3LYP/6-311++G (d,p) absolute energies (E, in a.u), relative energies (ΔE, in a.u) of the neutral and protonated forms of Thiotepa and Tepa in gas phase

Compounds	E	ΔE
Thiotepa	−1139.542981	0.356247
N-protonated Thiotepa	−1139.899228	0
S-protonated Thiotepa	−1139.884858	0.01437
Tepa	−816.575876	0.368897
N-protonated Tepa	−816.933435	0.011338
O-protonated Tepa	−816.944773	0

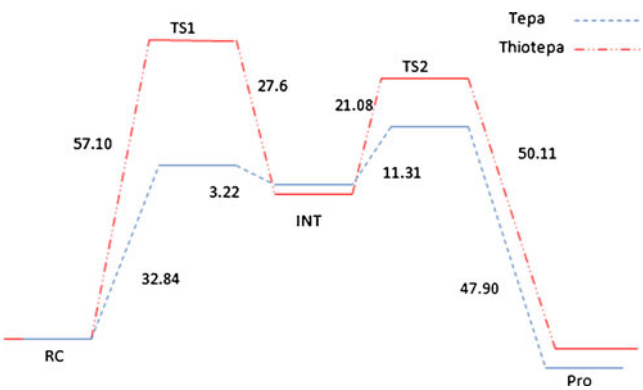

Fig. 8 The schematic potential energy surface of tepa and thiotepa hydrolysis in associative stepwise mechanism

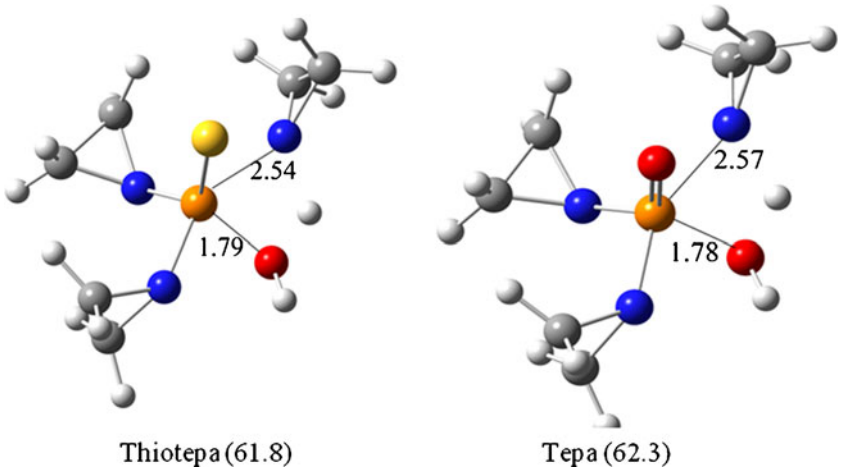

Fig. 9 Optimized geometries of transition state for tepa and thiotepa hydrolysis in gas phase in concerted front-side mechanism. Values in parentheses are Gibbs free energies of activation in kcal mol^{-1} for transition states in gas phase at 298 K (the bond distances are in Å)

good electrophile atom, which can interact attractively with negative sites on other molecules [68]. Therefore, this strong positive region on phosphorus atom of Thiotepa and Tepa can be a driving force for the backside attack mechanism.

AIM analysis shows that in reactant of Tepa (RC Tepa) there is weak hydrogen bonding ($\nabla^2 \rho(r)$ and H(r) >0) between H atom of water molecules with O atom on Tepa (11.7 kcal mol^{-1}). When H_2O molecule attacks phosphorous central atom, this hydrogen bond becomes weaker in transition state (8.1 kcal mol^{-1}). On the other hand, the $\rho(r)$ and E_X values for interaction between P atom and N atom of leaving group in transition state are lower that these values in reactant, which confirms this mechanism (for more details, see Table 3S). Similar results are obtained from AIM analysis for Thiotepa, but it is worth mentioning that there are no hydrogen bonds in Thiotepa in comparison with oxo analogue and the weak interaction between S atom on Thiotepa and H atom of H_2O molecule remains approximately stable in reactants and transition state. It is important to note that the new bond critical points between phosphorous atom and oxygen atom of H_2O molecule are observed in transition state for both agents. These results confirm the formation of a new bond in transition state (for more details, see Table 3S).

As mentioned previously, the acidic pH of cancer cells causes different behavior of these drugs in their treatment procedure, therefore the proton affinity (PA) of these two drugs were calculated to understand whether these drugs remain protonated or unprotonated under the acidic conditions. The PA results for Thiotepa and Tepa (225.0 and 225.8) show that both of them can accept the proton, therefore their hydrolysis in acidic pH can proceed by two other mechanisms (Fig. 5 and Fig. 6), which are investigated in 1.5 and 1.6 sections.

Acid–catalyzed concerted backside mechanism

Based on the lower activation barrier of the backside over the front side mechanism which is calculated for the unprotonated species, backside mechanism is the kinetically most probable mechanism. In addition, the steric effects for both unprotonated and protonated hydrolysis are supposed to be similar. Therefore, only the backside mechanism for the protonated P-N bond hydrolysis is investigated. The P-N bond distances in the ground state of N-protonated Thiotepa and Tepa, are 0.16 Å and 0.14 Å longer than those in the unprotonated species, respectively (i.e., 1.85 Å vs. 1.69 Å for Thiotepa, 1.82 Å vs. 1.68 Å for Tepa). On the other

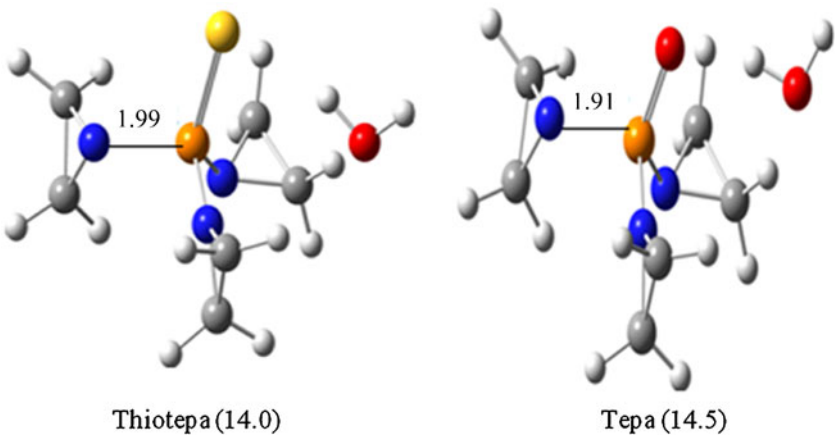

Fig. 10 Optimized geometries of stationary points for tepa and thiotepa hydrolysis in gas phase in concerted backside mechanism. Values in parentheses are Gibbs free energies of activation in kcal mol^{-1} for transition states in gas phase at 298 K (the bond distances are in Å)

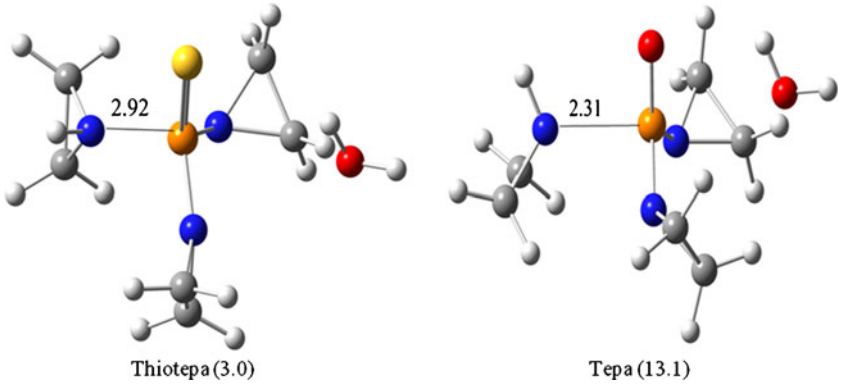

Fig. 11 Optimized geometries of stationary points for tepa and thiotepa hydrolysis in gas phase in acid-catalyzed backside mechanism. Values in parentheses are Gibbs free energies of activation in kcal mol^{-1} for transition states in gas phase at 298 K (the bond distance is presented in Å)

hand, in the transition state presented in Fig. 11, the P-N bond distance is 0.93 and 0.4 Å longer than those in the unprotonated mechanism for Thiotepa and Tepa, respectively (i.e., 2.92 Å vs. 1.99 Å for Thiotepa, 2.31 Å vs. 1.91 Å for Tepa). In addition, the free energy of activation in gas phase for protonated P-N bond hydrolysis for Thiotepa (3.0 kcal mol^{-1}, Fig. 11) and Tepa (13.1 kcal mol^{-1}, Fig. 11) are exactly 11 kcal mol^{-1} and 1.4 kcal mol^{-1} lower than those for the unprotonated mechanism, respectively. Therefore, it is obvious that the hydrolysis on protonated species is more rapid than the unprotonated species. This is rationalized by the presence of a good leaving group of aziridinuim.

NBO analysis was also carried out for this suggested mechanism. In the case of Tepa, there is strong hyperconjugation interaction between bonding orbital of $P\text{-}N_{(H)}$ and antibonding orbital of $P\text{-}O_{(Tepa)}$ (77.8 kcal mol^{-1}) in reactant. However, this value decreases to 53.7 kcal mol^{-1} in transition state. This change reveals the fact that the $P\text{-}N_{(H)}$ bond becomes weaker in transition state.

The AIM calculation also confirms these NBO results. The value of $E_{(x)}$ for $P\text{-}N_{(H)}$ bond decreases from 74.6 in reactant to 2.1 kcal mol^{-1} in transition state (see Table 4S for more details). Moreover, there is weak hydrogen bonding in reactant between H atom of H_2O molecule with oxygen atom on Tepa which becomes weaker in transition state. Moreover, based on AIM results the new critical point is observed between $O_{(H2O)}$ and P atom, implying formation of a new bond in transition state. Similar interactions are observed for Thiotepa by NBO and AIM analyses, but there are some differences between these two agents. Firstly, the interaction between P and $N_{(H)}$ is stronger in Tepa reactant which is indicated by shorter bond distance in comparison with Thiotepa. Secondly, there is no hydrogen bonding in the case of thio analogue (for more details, see Table 4S).

Acid–catalyzed dissociative stepwise mechanism

It is worth mentioning that in some experimental studies, the dissociative stepwise mechanism, or the corresponding acid-catalyzed dissociative mechanism, respectively, was proposed to be favored for tetracoordinate phosphorusamides that are structurally similar to Tepa and Thiotepa; including phosphoramide [61, 63–66]. Our calculations support this hypothesis for P-N bond hydrolysis of these two agents. Therefore, in addition to backside mechanism, the dissociative mechanism is investigated for protonated species because the aziridinuim ring is a good leaving group vs neutral aziridine ring. The $\Delta G^{\#}_{(g)}$ of transition state for Tepa and Thiotepa are 30.5 and 22.3 kcal mol^{-1}, respectively. The structures of transition states are presented in Fig. 12. In the transition state, the P-N bond distances in Thiotepa and Tepa are 3.03 and 3.07 Å, respectively.

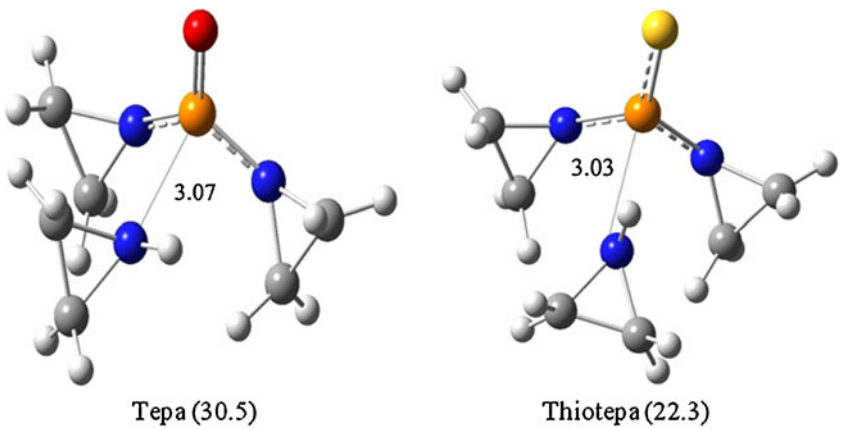

Fig. 12 Optimized geometries of stationary points for tepa and thiotepa hydrolysis in gas phase in acid-catalyzed dissociative stepwise mechanism. Values in parentheses are Gibbs free energies of activation in kcal mol^{-1} for transition states in gas phase at 298 K (The bond distance is presented in Å)

Table 3 The calculated activation free energies in gas phase and three different solution phases. The values are in kcal mol^{-1}

Mechanism	Compound		$\Delta G^{\#}_{(g)}$	$\Delta G^{\#}_{(aq)}$	$\Delta G^{\#}_{(THF)}$	$\Delta G^{\#}_{(DE)}$
Associative mechanism (neutral condition)	Thiotepa	TS1	57.1	58.4	57.7	57.1
		TS2	21.1	22.5	21.0	21.1
	Tepa	TS1	32.8	34.9	32.7	32.8
		TS2	11.3	13.1	11.2	11.8
Backside attack (neutral condition)	Thiotepa		14.0	14.2	13.9	13.6
	Tepa		14.5	14.9	14.6	14.2
Backside attack (acidic condition)	Thiotepa		2.9	2.1	2.9	3.0
	Tepa		13.1	13.3	13.6	13.5
Dissociative mechanism (acidic condition)	Thiotepa		22.3	18.6	17.1	17.2
	Tepa		30.5	28.7	25.3	26.7

The bond length which increases in transition states is rationalized by NBO analysis. Natural bond orbital analysis shows that in reactant there are strong hyperconjugation interactions between bonding orbitals of N-H $_{Thiotepa}$ and antibonding orbitals of P-S $_{Thiotepa}$. For example, $\sigma_{N\text{-}H\ Thiotepa}$ participates as donors and σ^{*} of P-S $_{Thiotepa}$ as acceptors with second order energy of 73.2 kcal mol^{-1}, while in transition state structure, the second order energy of $n \rightarrow \sigma^{*}$ type of interactions is $n_{N\text{-}H\ Thiotepa} \rightarrow \sigma^{*}_{P\text{-}S\ Thiotepa}$ (3.6 kcal mol^{-1}), which indicates weak hyperconjugation in transition state. There are similar interactions in Tepa, $\sigma_{N\text{-}H\ Tepa} \rightarrow \sigma^{*}_{P\text{-}O\ Tepa}$ is 75.3 kcal mol^{-1} in the reactant and 2.7 kcal mol^{-1} in the transition state. The reduction of interaction values in transition state for both agents (Thiotepa and Tepa) lead to increasing P-N bond lengths in transition state, and thus confirms that the hydrolysis mechanism in acidic condition can proceed via dissociative mechanism. Furthermore, the decrease of $E_{(X)}$ values for $N_{(az)}$-P bond in transition state for Thiotepa and Tepa (observed by the AIM analysis) confirms the results of NBO analysis. (See Table 5S for more details).

Solution phase

Consequently, the activation free energies and kinetic rate constants for all suggested hydrolysis mechanisms for Thiotepa and Tepa were calculated in three different solvents with the dielectric constant 80, 8, 4, using CPCM model. The values of activation free energies are presented in Table 3. In addition, Table 6S shows the kinetic rate constants values.

In the case of associative stepwise and backside mechanisms in neutral and acidic conditions, the barriers in these solvents are similar to those in gas phase due to the NBO charges and natural population analysis (NPA) values in reactant and transition states (see Table 7S-12S, for more details).

In acidic dissociation mechanism, water as a solvent has two different effects on reactant and transition state. On one hand, this polar solvent causes more stability of reactants due to localized charge on aziridinuim ring. On the other hand, water also can form hydrogen bond with hydrogen atom connected to the nitrogen atom of aziridinuim ring. It is important to note that hydrogen bonding stability is more

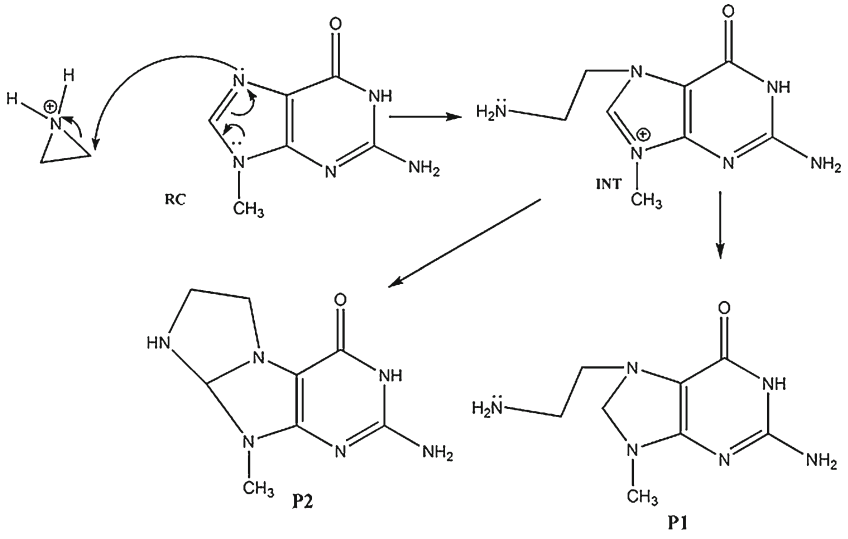

Fig. 13 The mechanism of reaction between aziridinuim ring and guanine

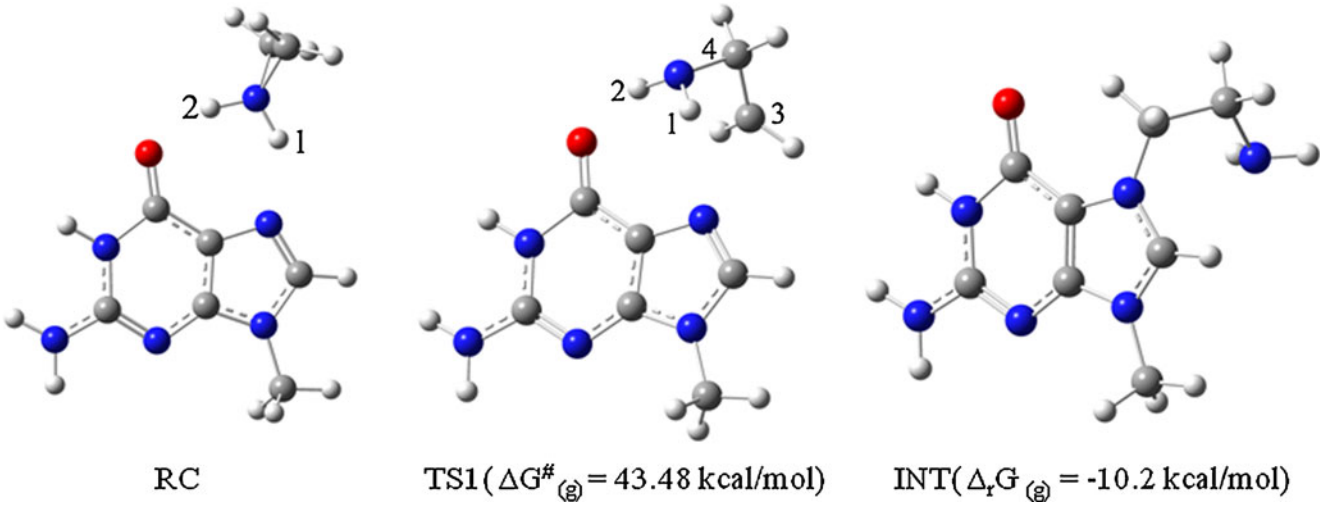

Fig. 14 The optimized structure of reaction coordinate (RC), transition state (TS1) and intermediate (INT) for second step

in transition state than in reactant because of the longer and weaker P-N bond in transition state. The reduction of values of barriers for Thiotepa and Tepa in water shows that the hydrogen bonding causes more stability of transition state and has more effect than the reactant due to polarity of solvent. Therefore, the barriers in water decrease.

In addition, THF and diethylether as nonpolar solvents have more effect on transition state due to distributed positive charge of aziridinuim ring. Therefore, transition state structure becomes stable and barriers reduce.

Second step: aziridine reaction

As mentioned in Introduction and several experimental studies, Thiotepa and Tepa are prodrug for aziridine (see pathway 2 from Fig. 2). In this way, Thiotepa and Tepa act as cell-penetrating carries for aziridine, which is released extracellulary after hydrolysis. The released aziridine can react with DNA on N7 site of Guanine nucleobase. Experimental studies introduce free aziridine as a weak base ($pK_{a\ (exp)}$=8.0) with high proton affinity ($PA_{\ (exp)}$=216.0 kcal mol^{-1}) [69, 70]. Hence, the protonated form of aziridine could exist at biological pH, forming electrophilic ions that have a positive charge on the nitrogen. Therefore, aziridinuim ion reacts with Guanine and produce two different products via the mechanism presented in Fig. 13.

Table 4 B3LYP/6-311++G (d,p) absolute energies (E, in a.u), Gibbs free energies (G, in a.u), relative energies (ΔE, in a.u), relative Gibbs free energies (ΔG, in a.u) of two different suggested products of second step

Products	E	ΔE	G	ΔG
P1	−716.971586	0	−717.028058	0
P2	−715.78392	1.187666	−716.249151	1.191636

It is well established that the rate-limiting step for reaction of the aziridine with the nucleophilic sites of DNA is the aziridine ring opening. In the first transition state (TS1, $\Delta G^{\#}_{\ (g)}$=43.48 kcal mol^{-1}, $k_{\ (g)}=6.33\times10^{-20}$ s^{-1}, see Fig. 14 for more details) of the this mechanism, the N7 as nucleophile in Guanine attacks the aziridine and causes the ring opening. The value of the Gibbs free energy is rationalized by the stability of reactant which is presented in Fig. 14. As shown in Fig. 14, the reactant becomes more stable because of hydrogen bonding between protons on the aziridinuim with oxygen and nitrogen atoms in Guanine. These hydrogen bonds are confirmed by the AIM analysis of which results are given in Table 13S.

Practically H2 $_{(az)}$-O $_{(Gua)}$ and H1 $_{(az)}$-N $_{(Gua)}$ hydrogen bonds in reactant are partly covalent, while H2 $_{(az)}$-O $_{(Gua)}$ in transition state is covalent (according to their -G(r)/V(r) ratio at the BCPs-see Table 13S in Supporting information for more details). Moreover, the results of AIM analysis revealed that weak hydrogen bonds such as H2 $_{(az)}$-O $_{(Gua)}$ in transition state show both $\nabla^2\rho(r)$ and H(r)>0, and medium hydrogen bonds show $\nabla^2\rho(r)$>0 and H(r) <0, while strong hydrogen bonds show both $\nabla^2\rho(r)$ and H(r) <0. Therefore, the both hydrogen bonds in the reactants are medium but it is important to note that H2 $_{(az)}$-O $_{(Gua)}$ (13.4 kcal mol^{-1}) are stronger than H1 $_{(az)}$-N $_{(Gua)}$ (8.4 kcal mol^{-1}). It is worth noting that the latter type of hydrogen bond was not observed in investigated systems (H1 and H2 are shown in Fig. 14).

Table 5 The kinetic data in different solvent for second step. ($\Delta G^{\#}$ in kcal mol^{-1} and k in s^{-1})

	$\Delta G^{\#}_{(aq)}$	$k_{(aq)}$	$\Delta G^{\#}_{(THF)}$	$k_{(THF)}$	$\Delta G^{\#}_{(DE)}$	$k_{(DE)}$
TS1	47.6	6.00×10^{-23}	46.6	3.00×10^{-22}	44.7	8.16×10^{-21}

Natural bond orbital analysis shows that in reactant there are strong hyperconjugation interaction between lone pairs of $N_{(Gua)}$ or $O_{(Gua)}$ atoms and antibonding orbitals of $N_{(az)}$. For example, $LP_{N(Gua)}$ and $LP_{O(Gua)}$ participate as donors and σ^* of $N_{(az)}$-H1 and $N_{(az)}$-H2 bonds as acceptors with second order energy of 18.6 and 27.7 kcal mol^{-1}, respectively. These values confirmed the results obtained from AIM analysis which predicts medium hydrogen bonding between H atoms of aziridinuim with O and N atoms on Guanine in reactant. In the case of transition state structure, the $n_{N(Gua)} \rightarrow \sigma^*_{N(az)\text{-}C3}$ interaction (38.2 kcal mol^{-1}) indicates $N_{(Gua)}$ as nucleophile attacks aziridinuim ring and causes the ring opening reaction (C3 is shown in Fig. 14).

The intermediate (INT, $\Delta_r G_{(g)}$=-10.2 kcal mol^{-1}, see Fig. 14 for more details) is an ionic compound which can undergo two different mechanisms. In one mechanism the intermediate yields main product of N7- ethylene amine guanine, which is believed to be a fast step. Another is the intramolecular cyclization which is not recognized experimentally. Rather, the intramolecular cyclization proceeds to form P2 (Fig. 13), as the product. The relative energies for these two different products via two different mechanisms are presented in Table 4. It is obvious from Table 4 that the P1 (N7- ethylene amine guanine) is more stable than another suggested product (P2) (for more details, see the Fig. 13). Therefore, the intramolecular cyclization mechanism becomes thermodynamically a disfavorable mechanism, even though it is possible kinetically. Consequently, further calculation on transition state of this mechanism was abandoned. It is important to note that these results are completely in accordance with the experimental observation of the N7- ethylene amine guanine (P1), as main alkylated product.

Solution phase

The rate constants and activation Gibbs free energies in different solvents with the dielectric constant of 80, 8 and 4 are presented in Table 5. In aqueous phase the activation free energy increases to 47.6 kcal mol^{-1}, which is rationalized by two parallel affects of water on stability of reactant. First, the reactant becomes more stable than transition state because of strong hydrogen bonding between aziridinuim ring and water molecules of solvent in reactant. Second, water as a polar solvent has more effect on reactant due to localized charge on aziridinuim ring. Therefore, these two effects cause more stability of reactant and increase of barrier. The positive charge, which is localized in reactant, is distributed in transition state during the proceeding of mechanism. Therefore the nonpolar solvents has more effect on transition state and causes more stability of transition state. Hence, the activation free energies decrease in comparison with its value in aqueous phase.

Conclusions

The activation free energies of P-N bond hydrolysis and their mechanisms in gas phase and solution phase were computationally evaluated and compared. The dissociative stepwise mechanism in physiological pH has the highest free energy, implying that it has no contribution to the total rate of hydrolysis.

Based on the calculated activation free energies of the concerted frontside mechanism and the stepwise associative mechanism (>50 kcal mol^{-1}), although they are kinetically more favorable than the dissociative stepwise mechanism, they have an insignificant role in the hydrolysis of P-N bond except in the case of Tepa in associative stepwise mechanism in which the activation free energy is 32 kcal mol^{-1} and it can be considered as a probable mechanism. However, our calculations indicate the concerted backside mechanism is the main pathway of Thiotepa and Tepa hydrolysis.

The dissociative mechanism for N-protonated species is the kinetically most favorable P-N bond hydrolysis mechanism for Thiotepa and Tepa in acidic pH, because free energy of activation is 55 kcal mol^{-1} lower than that for the unprotonated species. Although dissociative stepwise mechanism in acidic pH has suitable activation free energy for Thiotepa and Tepa and it can be considered as a probable mechanism, the barrier of acid-catalyzed concerted backside mechanism is estimated to be approximately 20 kcal mol^{-1} lower than the dissociative stepwise mechanism for both agents.

The predictive strategy presented here can in general be applied to prediction of a suitable mechanism of anticancer drugs.

Acknowledgments Support from Sharif University of Technology is gratefully acknowledged.

References

1. Sykes M, Karnofsky D, Phillips F, Burchenal JH (1953) Clinical studies of triethylene-phosphoramide and diethylene-phosphoramide compounds with nitrogen mustard-like activity. Cancer 6:142–148
2. Jones HC, Swinney J (1961) Thiotepa in the treatment of tumors of the bladder. Lancet 2:615–618
3. Perloff M, Hart RD, Holland JF (1977) Vinblastine, adriamycin, thiotepa and halotestin (VATH): therapy for advanced breast cancer refractory to prior therapy. Cancer 39:1289–1293
4. Gutin PH, Levi JA, Wiernik PH, Walker MD (1977) Treatment of malignant meningeal disease with intrathecal thiotepa: a phase II study. Cancer Treat Rep 61:885–887
5. Herzig GP (1987) High-dose ThioTEPA and autologous marrow transplantation: advances in cancer chemotherapy. Wiley, New York
6. Van Maanen MJ, Smeets CJM, Beijnen JH (2000) Chemistry, pharmacology and pharmacokinetics of N, N′, N″ - triethylenethiophosphoramide (ThioTEPA). Cancer Treat Rev 26:257–268

7. Van Maanen MJ, Tijhof IM, Damen JMA et al (1999) A search for new metabolites of N, N′, N″-triethylenethiophosphoramide. Cancer Res 59:4720–4724
8. Van Maanen MJ, Doesburg Smits K, Damen JMA et al (2000) Stability of Thiotepa and its metabolites, TEPA, monochloroTEPA and thioTEPA-mercapturate, in plasma and urine. Int J Pharm 200:187–194
9. Van der Wall E, Beijnen JH, RoDEnhuis S (1995) High-dose chemotherapy regimens for solid tumors. Cancer Treat Rev 21:105–132
10. Bestian H (1950) Uber einige reaktionen des aethylen-imins. Liebig's Annin Chemie 566:210–229
11. Maxwell J, Kaushik DS, Butler CG (1974) Behavior of an aziridine alkylating agent in acid solution. Biochem Pharmacol 23:168–170
12. Pyatigorskaya TL, Zhilkova OY, Shelkovsky VS et al (1987) Hydrolysis of 1,1′,1″-phosphinothioylidine trisaziridine (thioTEPA) in aqueous solution. Biomed Environm Mass Spectrom 14:143–148
13. Murray KM, Erkkila D, Gombotz WR et al (1997) Stability of thioTEPA (lyophilised) in 0.9% sodium chloride injection. Am J Health-Syst Pharm 54:2588–2591
14. Kolman A, Chovanec M, Osterman Golkar S (2002) Genotoxic effects of ethylene oxide, propylene oxide and epichlorohydrin in humans: update review (1990–2001) Mutat Res/Rev. Mutat Res 512:173–194
15. Farmer PB, Shuker DEG (1999) What is the significance of increases in background levels of carcinogen-derived protein and DNA adducts? Some considerations for incremental risk assessment Mutat Res/Fundam Mol Mech Mutagen 424:275–286
16. Kranjc A, Mavri J (2006) Guanine alkylation by ethylene oxide: calculation of chemical reactivity. J Phys Chem A 110:5740–5744
17. Benigni R, Bossa C (2010) Mechanisms of chemical carcinogenicity and mutagenicity: a review with implications for predictive toxicology. Chem Rev 111:2507–2536
18. Pullman B (1980) Carcinogenesis: fundamental mechanisms and environmental effects. D Reidel, Dordrecht, The Netherlands, pp 51–55
19. La DK, Swenberg JA (1996) DNA adducts: biological markers of exposure and potential applications to risk assessment. Mutat Res 365:129–146
20. LoPachin RM, DeCaprio AP (2005) Protein adduct formation as a molecular mechanism in neurotoxicity. Toxicol Sci 86:214–225
21. Ho TL (1975) Hard soft acids bases (HSAB) principle and organic chemistry. Chem Rev 75:1–20
22. Carlson RM (1990) Assessment of the propensity for covalent binding of electrophiles to biological substrates. Environ Health Perspect 87:227–232
23. Dunn JA, Bardos TJ (1991) Comparative chemical and biological studies of four prototype phosphoraziridine antineoplastic agents. Biochem Pharmacol 41:885–892
24. Hargreaves RHJ, Hartley JA, Butler J (2000) Mechanism of action of Quinone-containing alkylating agents: DNA alkylation by Aziridinylquinones. Front Biosci 172:172–180
25. Musser SM, Pan SS, Egorin MJ et al (1992) Alkylation of DNA with aziridine produced during the hydrolysis of N, N′, N″-triethylenethiophosphoramide. Chem Res Toxicol 5:95–99
26. Hemminki K (1984) Reactions of ethyleneimine with guanosine and deoxyguanosine. Chem Biol Interact 48:249–260
27. Egorin MJ, Snyder SW, Pan SS, Daly C (1989) Cellular transport and accumulation of thiotepa in murine, human, and avian cells. Cancer Res 49:5611–5617
28. Phillips RM, Bibby MC, Double JA (1988) Experimental correlations of in vitro drug sensitivity with in vivo responses to thiotepa in a panel of murine colon tumors. Cancer Chemother Pharmacol 21:168–172
29. Miller B, Tenenholz T, Egorin MJ et al (1988) Cellular pharmacology of N, N′, N″-Triethylenethiophosphor amide. Cancer Lett 41:157–168
30. Abraham TW, Kalman TI, McIntee EJ, Wagner CR (1996) Synthesis and biological activity of aromatic aminoacid phosphoramidates of 5-fluoro-20-deoxyuridine and 1-β-arabinofuranosylcytosine: evidence of phosphor-amidase activity. J Med Chem 39:4569–4575
31. Galesa K, Bren U, Kranjc A, Mavri J (2008) Determination carcinogenicity of acrylamide: a computational study. J Agric Food Chem 56:8720–8727
32. Warshel A (1991) Computer modeling of chemical reactions in enzymes and solutions. Wiley, New York
33. Miertus S, Scrocco E, Tomasi J (1981) Electrostatic interaction of a solute with a continuum. A direct utilization of ab initio molecular potentials for the prevision of solvent effects. Chem Phys 55:117–129
34. Pliego JR, Riveros JM (2001) The cluster-continuum model for the calculation of the solvation free energy of ionic species. J Phys Chem A 105:7241–7247
35. Spartan (2006) Spartan V102'; Wavefunction, Inc. Irvine, CA
36. Becke AD (1993) Density-functional thermochemistry. III The role of exact exchange J Chem Phys 98:5648–5652
37. Lee C, Yang W, Parr RG (1988) Development of the Colle-Salvetti correlation-energy formula into a functional of the electron density. Phys Rev B 37:785–789
38. Cossi M, Barone V, Mennucci B, Tomasi J (1998) *Ab initio* study of ionic solutions by a polarizable continuum dielectric model. Chem Phys Lett 286:253–260
39. Cossi M, Rega N, Scalmani G, Barone V (2003) Energies, structures, and electronic properties of molecules in solution with the C-PCM solvation model. J Comput Chem 24:669–681
40. Namazian M, Halvani S, Noorbala MR (2004) Density functional theory response to the calculations of pK_a values of some carboxylic acids in aqueous solution. J Mol Struct THEOCHEM 711:13–18
41. Sevastik R, Himo F (2007) Quantum chemical modeling of enzymatic reactions: the case of 4-oxalocrotonate tautomerase. J Bioorg Chem 35:444–457
42. Georgieva P, Himo F (2008) Density functional theory study of the reaction mechanism of the DNA repairing enzyme alkylguanine alkyltransferase. Chem Phys Lett 463:214–218
43. Chen S, Fang w, Himo F (2008) Technical aspects of quantum chemical modeling of enzymatic reactions: the case of phosphotriesterase. Theor Chem Account 120:515–522
44. Himo F, Guo J, Rinaldo-Matthis A, Nordlund P (2005) Reaction mechanism of deoxyribonucleotidase: a theoretical study. J Phys Chem B 109:20004–20008
45. Pliego JR (2004) Basic hydrolysis of formamide in aqueous solution: a reliable theoretical calculation of the activation free energy using the cluster-continuum model. Chem Phys 306:273–280
46. Stare J, Henson NJ, Eckert J (2009) Mechanistic aspects of propene epoxidation by hydrogen peroxide. Catalytic role of water molecules, external electric field, and zeolite framework of TS-1. J Chem Inf Model 49:833–846
47. Nguyen MT, Raspoet G, Vanquickenborne LG (1999) Necessity to consider a three-water chain in modelling the hydration of ketene imines and carbodiimides. J Chem Soc 4:813–820
48. Reed AE, Weinhold F (1985) Natural localized molecular orbitals. J Chem Phys 83:1736–1740
49. Reed AE, Weinstock RB, Weinhold F (1985) Natural population analysis. J Chem Phys 83:735–746
50. Reed AE, Weinhold F (1983) Natural bond orbital analysis of near–Hartree–Fock water dimer. J Chem Phys 78:4066–4073
51. Foster JP, Weinhold F (1980) Natural hybrid orbitals. J Am Chem Soc 102:7211–7218
52. Chocholousova J, Vladimir Spirko V, Hobza P (2004) First local minimum of the formic acid dimer exhibits simultaneously red-

shifted O–HO and improper blue-shifted C–HO hydrogen bonds. Phys Chem Chem Phys 6:37–41
53. Reed AE, Curtiss LA, Weinhold F (1988) Intermolecular interactions from a natural bond orbital, donor-acceptor viewpoint. Chem Rev 88:899–926
54. Bader RFW (2002) AIM2000 program package, Ver. 2.0, McMaster University: Hamilton, Ontario, Canada
55. Bader RFW (1998) Bond Path: a universal indicator of bonded interactions. J Phys Chem A 102:7314–7323
56. Bader RFW (1990) Atoms in molecules. A quantum theory. Clarendon, Oxford, UK
57. Pakiari AH, Eskandari K (2006) The chemical nature of very strong hydrogen bonds in some categories of compounds. J Mol Struct THEOCHEM 759:51–60
58. Abboud JLM, Mó O, De Paz JLG et al (1993) Thiocarbonyl versus carbonyl compounds: A comparison of intrinsic reactivities. J Am Chem Soc 115:12468–12476
59. Hocquet A (2001) Intramolecular hydrogen bonding in 2′-deoxyribonucleosides: an AIM topological study of the electronic density. Phys Chem/Chem Phys 3:3192–3199
60. Rozas I, Alkorta I, Elguero J (2000) Behavior of ylides containing N, O, and C atoms as hydrogen bond acceptors. J Am Chem Soc 122:11154–11161
61. Rahil J, Haake P (1981) Reactivity and mechanism of hydrolysis of phosphonamides. J Am Chem Soc 103(1723):1734
62. Ganta S, Devalapally H, Shahiwala A, Amiji M (2008) A review of stimuli-responsive nanocarriers for drug and gene delivery. J Con Rel 126:187–204
63. Chanley JD, Feageson E (1963) A study of hydrolysis of phosphoramides. II Solvolysis of phosphoramidic acid and comparison with phosphate esters J Am Chem Soc 85:1181–1190
64. Garrison AW, Boozer CE (1968) The acid-catalyzed hydrolysis of a series of phosphoramidates. J Am Chem Soc 90:3486–3494
65. Koizumi T, Haake P (1973) Acid-catalyzed and alkaline hydrolyses of phosphinamides. The lability of phosphorus-nitrogen bonds in acid and mechanisms of reaction J Am Chem Soc 95:8073–8079
66. Richter S, Teopelmann W, Lehmann HA (1976) Hydrolysis of phosphoric acid amides. Z Anorg Allg Chem 424:133–143
67. Haake P, Koizumi T (1970) Hydrolysis of phosphinamides and nature of P-N bond. Tetrahedron Lett 55:4845–4848
68. Murray JS, Lane P, Politzer P (2009) Expansion of the -hole concept. J Mol Model 15:723–729
69. Rozeboom MD, Houk KN, Searles S, Seyederzai SE (1982) Photoelectron spetroscopy of N-aryl cyclic amines. Variable conformations and relationships to gas and solution phase basicities. J Am Chem Soc 104:3448–3453
70. Lias SG, Liebman JF, Levin RD (1984) Evaluated gas phase basicities and proton affinities of molecules; heats of formation of protonated molecules. J Phys Chem (ref data) 13:695–808